Quantitative Analysis of Chemoconvection Patterns in the Methylene-Blue−Glucose System

A. J. Pons,*,† F. Sagués,‡ M. A. Bees,§ and P. G. Sørensen||

Department of Chemistry, H. C. Ørsted Institute, University of Copenhagen, Universitetsparken 5, DK-2100 Copenhagen, Denmark, Departament de Química Física, Universitat de Barcelona, Martí i Franqués 1, 08028 Barcelona, Spain, and Department of Mathematics and Statistics, University of Surrey, Guildford, GU2 7XH, U.K.

Received: November 29, 2001; In Final Form: March 19, 2002

We report a quantitative analysis of a series of chemically induced convection patterns for the methylene-blue−glucose system at different experimental conditions. The objective of the study is to get some quantitative knowledge of the phenomenon (for example, the characteristic wavelength and the characteristic time for the pattern to appear). We focus our attention on the initial stages of the pattern appearance just after the instability and at some aspects of the general behavior of the complete pattern evolution. We analyze the effect on length and time scales of the patterns obtained when varying the initial values of three different experimental parameters (viscosity, pH, and layer depth). The results obtained in the "linear growth" regime reproduce the qualitative trends extracted from the linear stability analysis of a theoretical model subject to a pseudo-steady-state approximation.

1. Introduction

One of the most extensively studied hydrodynamic instabilities is that associated with the Rayleigh−Bénard convection.[1] It can occur when a layer of fluid is heated from below. If the temperature difference between the top and bottom boundaries is sufficiently large, a set of convection cells appear in the layer. Besides this paradigmatic example, many other instabilities occur in hydrodynamic settings, such as the Rayleigh−Taylor instability[1,2] (appearing when a dense fluid is placed on top of a lighter one), the Taylor−Couette instability[3] (resulting when a fluid is placed between two coaxial cylinders that are rotating at sufficiently different angular velocities) or the Saffman−Taylor instability[4] (appearing when two fluids of different viscosity are pushed one into the other by a pressure gradient through a Hele−Shaw cell). Many examples of chemically induced instabilities appear in reaction−diffusion systems. The most extensively studied chemical instabilities are found in the Belousov−Zhabotinsky reaction, giving rise to target patterns, spirals, or scrollwaves, etc.,[5] or in other autocatalytic schemes, like the CIMA reaction showing Turing-like patterns.[6] In fields such as biology, there exist patterns ranging from those observed in the growth of bacterial colonies[7] to tissues.[8] Closer to our interests, here, one type of pattern appears in the context of biofluid dynamics called bioconvection,[9] due to its similarity with convection. The pattern appears as a consequence of an instability arising from aggregations of swimming microorganisms, which are produced by a variety of mechanisms. For instance, some cells tend to swim upward on average (e.g., due to the mass distribution within cells, gradients in light intensity or gradients in oxygen) which may result in aggregations at an upper free surface, or within a specific region of the flow field due to competing torques acting on the cell. A gravitational instability occurs when the aggregating microorganisms are of a different density to the fluid in which they swim. In particular, a suspension of microorganisms that tend to swim upward eventually produces a density profile determined by a balance of diffusive and motile effects.[10] If this profile has a sufficiently large gradient, then fluid circulation results. In this paper, we study a chemical system for which the behavior is similar to bioconvective systems. In this case the instability is called "chemoconvection" and the unstable density profile is built not by the aggregation of organisms, but by the concentration of a dense product of a set of chemical reactions.[11,12]

Many chemoconvective patterns have been studied previously. Some examples are shown in[13,14] where a variety of experimental scenarios are considered including the chemical system we are referring to in this paper.

If glucose (GL), sodium hydroxide (NaOH), oxygen (O_2), and methylene-blue are mixed in water, for an appropriate range of concentrations, a set of chemical reactions will occur.[15,16] This mixture is sometimes known as "the blue bottle experiment". The set of reactions taking place can be summarized by saying that glucose and oxygen, in a basic medium, are converted to gluconic acid (GLA) with methylene-blue working as a catalyst (see ref 17 for a full description of the reactions):

$$O_2 + 2\mathrm{MBH} \rightarrow 2\mathrm{MB}^+ + 2\mathrm{OH}^- \quad (1)$$

$$\mathrm{GL} + \mathrm{MB}^+ + \mathrm{OH}^- \rightarrow \mathrm{MBH} + \mathrm{GLA} \quad (2)$$

The catalyst (methylene-blue) is present in the reaction in two main forms: the blue oxidized form MB^+ and the colorless reduced form MBH. The oxidation of the methylene-blue, in reaction 1, is much faster than its reduction, produced in reaction 2. So the conversion of the blue (oxidized) form into the colorless (reduced) form of methylene-blue is the rate-limiting process of the oxidation of glucose to gluconic acid. The reaction

† University of Copenhagen and Universitat de Barcelona. E-mail: apr@kiku.dk. E-mail: a.pons@qf.ub.es.

‡ Departament de Química Física, Universitat de Barcelona. E-mail: f.sagues@qf.ub.es.

§ Department of Mathematics and Statistics, University of Surrey. E-mail: m.bees@surrey.ac.uk.

|| Department of Chemistry, H. C. Ørsted Institute, University of Copenhagen. E-mail: pgs@kiku.dk.

10.1021/jp014346n CCC: $22.00
Published on Web 06/27/2002

rates of the two chemical equations are k_1 and k_{obs}, respectively. See ref 11 for a full description of the kinetic model and the methods used to measure the rate constants of both reactions. In that paper, the range of patterns obtained were investigated while varying parameters, such as the initial concentrations of the reacting species, temperature, and layer depth of the fluid. Furthermore, many similar patterns can be obtained using other saccharides and indicators.[18,19]

One mechanism that could explain the instability that produces the pattern is discussed and analyzed in ref 12. Following the hypothesis contained therein, the pattern is formed as follows. We pour a solution composed of methylene-blue, glucose, and sodium hydroxide, which has been previously shaken to be saturated with oxygen, into a Petri dish placed in a thermostatic chamber. The fluid is initially blue due to reaction 1 and at rest. As time goes on, it reacts at the rate imposed by reaction 2 consuming the oxygen diluted in the solution and glucose to produce gluconic acid. Since there is a continuous supply of oxygen into the fluid from the upper surface, which is in contact with the atmosphere, the concentration of oxygen in the upper part of the fluid is not depleted as fast as it is in the lower part of the layer. As a consequence, the concentration of the products, and hence gluconic acid, is higher in the upper part of the fluid than it is in the lower. It was shown in ref 11 that a solution of gluconic acid is denser than an equimolar solution of glucose. Thus the balance between reactive and diffusive processes leads to a top-heavy density profile, which eventually becomes unstable (Rayleigh−Taylor instability) and the fluid overturns. This happens between tens of minutes to hours after the fluid has been poured into the Petri dish. The down-welling fluid is blue because it comes from the upper parts of the fluid that is rich in oxygen. This results in circulation cells which are arranged mainly in lines or dots (see ref 11). They are composed of a sinking dark blue part and a surrounding lighter (eventually colorless) blue part rising from the bottom.

In this paper, we shall study quantitatively the images of patterns evolving from different initial conditions. The paper is organized as follows. In the following section, we make a remark on the experimental conditions employed to obtain the patterns and the procedures used to analyze the pictures. In section 3, we discuss a reference case, where we describe in detail the application of the techniques explained in section 2 and compare the experimental results with the theoretical predictions at the initial stages of the pattern evolution. Section 4 contains the bulk of the results and the discussion on the influence of viscosity, pH, and solution depth on the experimentally obtained patterns. Finally, in section 5 we discuss the results and the theoretical predictions.

2. Materials and Methods

2.1. Experimental Setup. Double ion-exchanged water was used throughout. NaOH (Merck A109956), analytical grade D(+)-glucose (Merck A108337), polyethylene oxide (BDH Chemicals Ltd., Poole, England, Polyox WSR-301, Prod 29740, MW approximately 4 000 000) and methylene blue (Fluka A55631) were used without further purification. Water, 1 M NaOH, 0.03126 M MB^+, glucose, and polyethylene oxide were mixed to obtain the desired concentrations. After the solution was thermostated for half an hour, it was shaken (to saturate the solution with oxygen) and poured into a Petri dish (inner diameter 18.5 cm and height 2.7 cm). During the experiments the Petri dish was inserted into a glass-plate-covered cylindrical container which was maintained at 19.0 °C ± 0.1 °C by a Heto CB 8−30 thermostat. The Petri dish was covered to prevent perturbations on the pattern produced by air movement and to saturate the air above the fluid with water and thus prevent evaporation. The system was homogeneously illuminated with a lamp from above. Pictures were taken periodically during the experiment by a computer-controlled CCD-9230 camera and stored electronically (see the scheme of the experimental setup in Figure 1 of ref 11). The width of all the images displayed here corresponds to 12.4 cm.

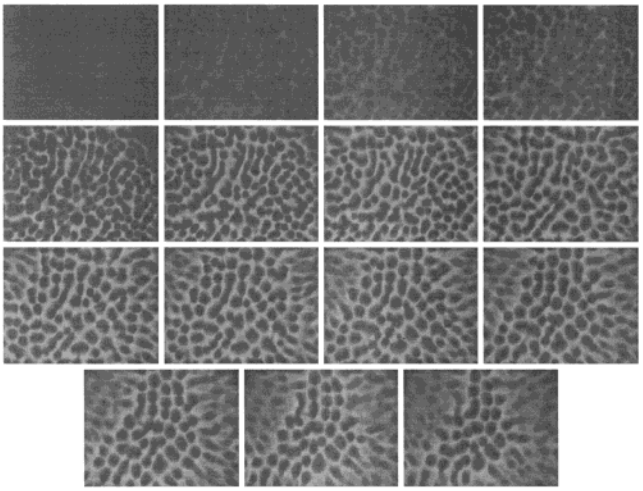

Figure 1. Time evolution for chemoconvection patterns corresponding to the reference experiment no. 12. The sequence of patterns correspond to the following times (in seconds), 250 (used as background), 3625, 3750, 3875, 4375, 5375, 6250, 8750, 10000, 11250, 12500, 13750, 15000, 16250, and 17500.

In Table 1 we summarize the conditions under which the experiments analyzed in this paper were performed. The conditions in experiment no. 0 define what we call the standard conditions (s.c.). Experiment no. 12 is employed in section 3 as a reference case to illustrate the application of the techniques explained in the next subsection.

In the first block of experiments we vary the initial concentration of polyethylene oxide (PEO). An increase of its concentration considerably increases the viscosity of the system without affecting appreciably its chemistry (in the range of concentrations used for the experiments). Since concentration changes the viscosity, it controls the Rayleigh number of the system with a negligible effect on the rest of the nondimensional parameters (see their definition in Tables 2 and 3, and details in ref 12). The second block of experiments corresponds to variations in the initial concentration of NaOH. This is the chemical parameter that significantly affects the chemistry of the system and, as was seen in ref 11, it has a considerable influence on the patterns that appear in the system. The changes of the initial concentrations of the other compounds have much less influence on the patterns, as was also shown in ref 11. The third block of experiments corresponds to changes in layer depth. This parameter alters the geometrical conditions of the system. Finally, we have not considered the influence of temperature on the patterns as this parameter changes the chemistry of the system and the viscosity and diffusivity of the species at the same time. Hence, it would be difficult to explain to which one of those changes we have to attribute the behavior observed at different temperatures.

2.2. Image Analysis Procedure. The study of the images follows closely the techniques used in Bees and Hill.[20,21] The characteristic wavelengths of the patterns were calculated using two-dimensional Fourier transforms generated by an image-processing software package, IDL (Research Systems Inc.,

TABLE 1: Description of the Experimental Conditions for the Experiments When Changing Initial Concentrations of Polyethylene Oxide, Initial Concentrations of NaOH, and Layer Depths[a]

no.	temp. (°C)	depth (cm)	s/picture	[NaOH] (M)	[MB^+] (M)	[GL] (M)	[PEO] (M)
0	19	0.8	25	0.02	4.6×10^{-5}	0.054	0
1	s.c.	s.c.	30	s.c.	s.c.	s.c.	1.5×10^{-7}
2	s.c.	s.c.	30	s.c.	s.c.	s.c.	3.0×10^{-7}
3	s.c.	s.c.	40	0.012	s.c.	s.c.	s.c.
4	s.c.	s.c.	30	0.020	s.c.	s.c.	s.c.
5	s.c.	s.c.	5	0.073	s.c.	s.c.	s.c.
6	s.c.	s.c.	4	0.098	s.c.	s.c.	s.c.
7	s.c.	s.c.	5	0.195	s.c.	s.c.	s.c.
8	s.c.	0.59	20	s.c.	s.c.	s.c.	s.c.
9	s.c.	0.68	30	s.c.	s.c.	s.c.	s.c.
10	s.c.	0.88	30	s.c.	s.c.	s.c.	s.c.
11	s.c.	1.17	20	s.c.	s.c.	s.c.	s.c.
12	18	s.c.	s.c.	s.c.	s.c.	s.c.	s.c.

[a] Experiment no. 12 describes the conditions of the reference experiment discussed in section 3. The values of the experimental parameters in boxes where "s.c." (for standard conditions) is written are the same as those for experiment no. 0.

Colorado, USA), on a workstation. We studied each series of images, which have 256 pixels × 192 pixels and 256 levels of gray. One of the pictures taken just after starting the experiment was used as a background image and it was subtracted from the whole series of pictures. By doing this we remove the inhomogeneities in the illumination that could influence the result of the FFT. Two bands of zeros were added to the images to produce pictures of size 256 pixels × 256 pixels (for optimization reasons when using the FFT algorithm). After applying a suitable Hann windowing function to the images, the FFT were made. We will use the discrete Fourier spectrum P_n defined on $N/2$ intervals (called bins) I_n as

$$P_n = \sum_{d(k_x,k_y)\in I_n} |H(k_x,k_y)|^2 \tag{3}$$

following Bees and Hill nomenclature.

Due to the fact that the structures that are involved in the pattern are not periodic at all but are distributed randomly in space and that a band of modes is excited when the pattern appears, the Fourier spectrum obtained will be formed, mainly, by a peak located over a range of wavenumbers. This peak will be characterized by its center and its width. As a consequence of this, an unnormalized Gaussian distribution, $G(x)$, was chosen to fit the Fourier spectrum:

$$G(x) = A_1 \exp\left[-\left(\frac{x+\mu_1}{\lambda_1}\right)^2\right] \tag{4}$$

where A_1, μ_1, and λ_1 are constants fitted to the data. The modes of wavenumber $k = 0$, 1, 2, and 3 are set equal to zero because they are associated to what is called the peak of energy of the whole image. Moreover, their weight in the fit is set to zero.

To study the appearance of the pattern and as a measure of its contrast, we calculate, following ref 22, standard deviation of the gray level

$$\sigma = \left(\frac{1}{N_p - 1}\sum_{j=1}^{N_p}(g_j - \bar{g})^2\right)^{1/2} \tag{5}$$

where N_p is the total number of pixels in each image, g_j is the level of gray of pixel j, and $\bar{g}$ is the average gray level. Furthermore, we also track the evolution in time of $\bar{g}$ and the time derivative of σ, $\dot{\sigma}$. To calculate the derivative numerically it is necessary to smooth the values of σ.

3. Reference Case

To show a typical example, we choose the following initial conditions for the experiment: $[OH^-] = 0.020$ M, $[MBH] + [MB^+] = 4.6 \times 10^{-5}$ M, [GL] = 0.054 M, depth ≈8 mm, and temperature = 18 °C (experiment no. 12). The evolution of the pattern can be followed in Figure 1. We can see, from this sequence of pictures, that the pattern is not steady. It evolves with time: the pattern emerges, develops, and finally, disappears.[11] Note, however, that the levels of gray are linked to the concentration of methylene-blue. This means that we are not monitoring directly the flow field, but the evolution of the distribution of methylene-blue. We assume that both fields have the same horizontal spatial periodicity. This assumption may be unjustified, for example, when a sinking "drop" of, initially, oxidized methylene-blue is being reduced due to reaction 2 during its sinking.

The behavior of the mixture after pouring it into the Petri dish is the following. At the beginning, the fluid is homogeneous and blue (the first picture is dark gray). During this time the chemical reactions are taking place, the medium is quiescent and the unstable profiles are developing. After a while, a pattern starts to appear; regions in light gray develop around regions in dark gray. In the reference case the pattern developed is dot shaped (see second picture). During the evolution of the pattern, the length scale of the patterns varies (see, for instance, pictures from time 4375 to 8750 s). Finally, the pattern disappears from the outside inward.

To estimate when the pattern appears we measure the evolution in time of the average gray level $\bar{g}$, its standard deviation (contrast) σ, and its time derivative $\dot{\sigma}$.[22] These data are displayed in Figure 2, where we can observe that the evolution in time of the average gray level and contrast show clearly the onset of the instability (when both start increasing). Actually, σ starts to increase at time ≈3100 s and we call this the onset time. Also, note that the maximum of $\dot{\sigma}$ appears at time 3900 s, which may be associated with the end of the "linear growth" regime. This measure is rather arbitrary, but it indicates a time when a relevant change of behavior in σ is made apparent and thus easy to establish. We define $t_{\max(\dot{\sigma})}$ as the time for the maximum of $\dot{\sigma}$. We have added two vertical lines to Figure 2 showing these two times.

In what follows, we will compare our results with theoretical predictions which follows from a pseudo-steady-state linear stability analysis.[12] The term "pseudo-steady-state" refers, as indicated in ref 12, to the fact that the linear stability analysis in our system is applied to a reference state consisting of a

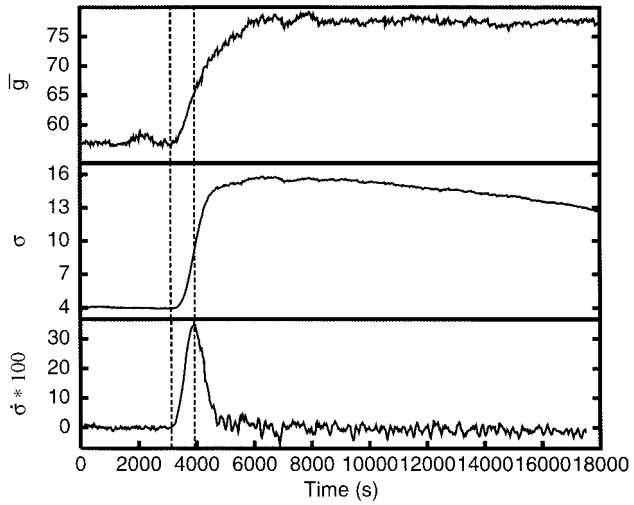

Figure 2. Evolution in time of different indicators of gray levels in the patterns (see text) $\bar{g}$, σ, and $\dot{\sigma}$. The lines correspond to the onset of the pattern (3100 s) and $t_{\max(\dot{\sigma})}$ (3900 s).

TABLE 2: Parameter Estimates and Experimental or Reference Values (with Appropriate s.f.) Corresponding to the Conditions for Reference Experiment No. 12

name	description	value or range	units
H	suspension depth	0.8	cm
D	diffusivity[a] of MBH and MB^+	4×10^{-6}	cm^2/s
D_A	diffusivity of GLA	6.7×10^{-6}	cm^2/s
D_Ω	diffusivity of oxygen	2.11×10^{-5}	cm^2/s
ρ	fluid density (∼water at 25 °C)	0.9970	g/cm^3
ρ_{GL}	solution density per M of GL	1.065 ± 0.009	g/cm^3
ρ_{GLA}	solution density per M of GLA	1.108 ± 0.009	g/cm^3
$\Delta\rho$	excess solution density per M of GLA (replacing M of GL) $= \rho_{GLA} - \rho_{GL}$	0.044 ± 0.018	g/cm^3 M
μ	dynamic viscosity	1.05×10^{-2}	g/cm s
ν	kinematic viscosity	1.053×10^{-2}	$cm^2/$ s
g	acceleration due to gravity	10^3	cm/s^2
k_1	fast reaction rate	2.675×10^3	/M s
k_{obs}	slow reaction rate	3.61×10^{-3}	/s
W_0	initial (homogeneous) concentration of MBH + MB^+	4.6×10^{-5}	M
Ω_0	concentration of O_2 at the free surface	2.6×10^{-4}	M
$\bar{H}$	sublayer depth $= (D/k_{obs})^{1/2}$	0.033	cm

[a] Parameter estimates.

TABLE 3: Nondimensional Parameters for Reference Experiment No. 12 Calculated Using the Values of Table 2

name	description	expression	value or range
d	scaled fluid depth	$H/\bar{H}$	24.0
κ	reaction ratio	$2k_1\Omega_0/k_{obs}$	385
λ	reaction ratio	k_1W_0/k_{obs}	34.1
δ	diffusion ratio	D_Ω/D	5.28
δ_A	diffusion ratio	D_A/D	1.68
R	Rayleigh number	$g\Delta\rho W_0\bar{H}^3/\mu D$	1.73
S_c	Schmidt number	ν/D	2632.5

continuously time evolving state of concentrations, free of convection, and homogeneous in the horizontal direction, rather than to strictly steady-state profiles. This is due to the open nature of the chemical system.

The characteristic time of growth, corresponding to the highest growth rate mode, decreases in time, as the unstable density profile becomes steeper. The theoretical onset time, can be estimated as the time when the characteristic time of growth is of the order of the natural time scale of the system ($\tau = k_{obs}^{-1} = 277.01$ s; see Tables 2 and 3). For the reference case, the onset time is calculated to be ≈3500 s, which is in very good agreement with the experimental value (≈3100 s).

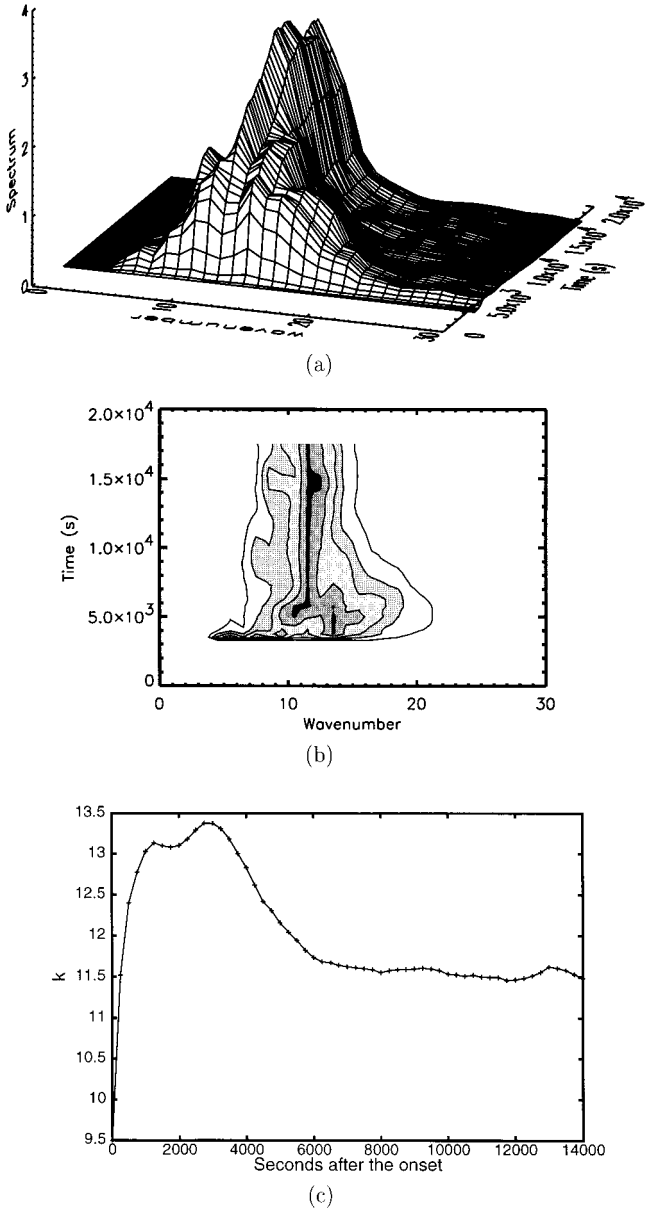

Figure 3. (a) Fourier spectrum versus time from data (experiment no. 12). (b) Levels of gray correspond to 97% (in black), 95%, 90%, 80%, 60%, 40%, and 20% of the highest value of the Fourier spectrum for that time, respectively. (c) Evolution in time of the center of the Gaussian fit to the experimental data. (Here, time 0 means time of the first picture for which the dominant peak of the Fourier spectrum is higher than the noise.) To recover the original time, an offset of 3500 s should be added.

Eventually, both $\bar{g}$ and σ stop growing, which means that the pattern contrast is not enhanced any more and nonlinear effects are progressively controlling the growth induced in the linear regime. In fact, it can be seen that σ slowly decreases, and the pattern slowly disappears. However, this fact does not necessarily mean that the fluid stops moving.

To study the general behavior of the length scales of the system for the whole range of times (from 3250 to 17500 s) we take every 10 pictures in order to reduce the computation time. In Figure 3a,b we show the evolution of the Fourier spectrum for the range of time indicated above. We can see that the initial behavior, where the characteristic wavenumber increases in time, is not the general one and that the magnitude of the power spectrum of the highest mode grows for some time, before decreasing (not shown). We observe, too, that the width of the

band of modes decreases, in general, after reaching a maximum value. The evolution of the fit reproduces this general behavior.

Figure 3c shows the evolution in time of the center of the Gaussian used to fit the data. At the beginning ("linear growth" regime) the wavenumber increases in time as predicted by the linear stability analysis.[12] The observation that the wavenumber increases is related with the fact that in the real space some dots break and some new dots develop in this regime between existing structures. At time ≈5000 s (which corresponds to 1500 s in abscissa of Figure 3c), a new regime appears when the wavenumber stops monotonically increasing and later on starts to decrease until time ≈10000 s (6500 s in abscissa of Figure 3c). In this regime there is an aggregation process that makes bigger dots from the small ones. The nonlinear effects are working to select a specific wavenumber while reducing the band of excited modes. This can be explained if the modes with higher wavenumber are damped in the nonlinear regime. This phenomenon is predicted in the Rayleigh−Bénard instability between insulating boundaries already within the weakly nonlinear regime.[23] In this example, the specific wavenumber ($k \approx 11.5$) is reached and stays for the rest of evolution. This last regime ranges from time ≈10000 s to time ≈17500 s, in which the pattern begins to disappear. The near constant value of the average gray indicates that when the dots disappear the oxidized form of the methylene-blue is distributed in the whole area and the fact that σ decreases slowly demonstrates that the contrast (the pattern) is disappearing. The three ranges can be identified qualitatively in terms of the shape of the patterns shown in Figure 1. The six first images correspond to the growth regime, the following three images correspond to the saturation regime and the last six images to the disappearance of the pattern. Similar regimes have been observed in systems subject to the Rayleigh−Taylor instability.

4. Quantitative Dependence of the Results on the Parameters

In this section we describe the results obtained when three different experimental parameters are changed. In particular, we study the influence on the basic time and length scales of the system.

4.1. Hydrodynamic Parameter: Viscosity. The main influence of PEO on the system parameters is to increase the viscosity. It will also influence the average density and the diffusivities of the different species, but we expect these effects to be small. We checked by experiments that the influence of PEO on the chemical reactions is negligible. We, thus, assume that the influence of PEO on the patterns can be explained by the change in the Rayleigh number by means of the kinematic viscosity (see Table 4).

In Figure 4 we present the shape of the patterns at a time corresponding to saturation of σ for increasing initial concentrations of PEO. It is not difficult to see that the dominant wavenumbers of the structures involved in the pattern are affected. It is clear, too, that the pattern become less contrasted as the concentration increases. This can be explained by the following reasoning. When the Rayleigh number is decreased by the increasing concentration of PEO (see Table 4), the system becomes unstable at a later time (see Figure 5). Hence, the chemical reactions, in that case, have been reducing the depth of the subsurface layer of blue (oxygen rich) fluid for a longer time. As a result, this blue subsurface layer is becoming shallower as time goes on and it appears lighter blue. When the pattern emerges later in an experiment, the dark regions of the pattern, that are composed of regions of sinking blue subsurface layer, are lighter than those produced when the pattern emerges earlier.

TABLE 4: Assumptions of the Changes Made in the Length and Time Scales and the Nondimensional Parameters Used to Interpret the Experimental Results[a]

name	description	expression	changing [PEO]	changing [NaOH]	changing depth (H)
$\bar{H}$	length scale	$(D/k_{obs})^{1/2}$	◇ (D)[a]	via k_{obs}	×
τ	time scale	k_{obs}^{-1}	×[b]	via k_{obs}	×
d	scaled fluid depth	$H/\bar{H}$	◇ (D)	via $\bar{H}$	via H
κ	reaction ratio	$2k_1\Omega_0/k_{obs}$	×	◇ (k_1, k_{obs})	×
λ	reaction ratio	k_1W_0/k_{obs}	×	◇ (k_1, k_{obs})	×
δ	diffusion ratio	D_Ω/D	◇ (D_Ω,D)	×	×
δA	diffusion ratio	D_A/D	◇ (D_A,D)	×	×
R	Rayleigh number	$g\Delta\rho W_0\bar{H}^3/\mu D$	via μ	via $\bar{H}$	×
S_c	Schmidt number	ν/D	◇ (μ,D)	×	×

[a] The symbol "◇ (...)" states that the experimental parameters specified in the parenthesis do change, but we assume that the specific nondimensional parameter has only a small influence compared to other nondimensional parameter changes. [b] The symbol "×" indicates that the corresponding nondimensional parameter does not change appreciably when the stated parameter is varied.

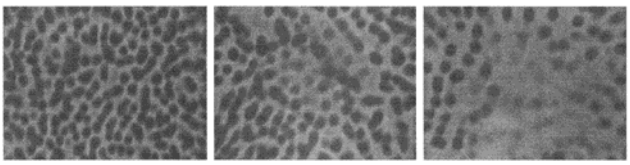

Figure 4. Typical patterns at a time corresponding to the saturation of contrast for increasing initial concentrations of PEO.

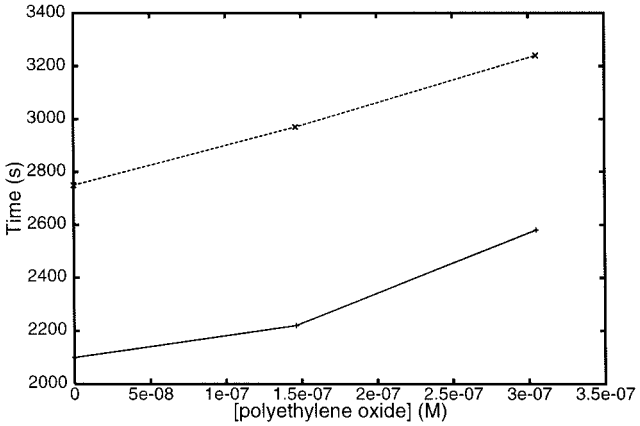

Figure 5. Times for the onset (solid line) and $t_{max(\dot{\sigma})}$ (dashed line) versus the initial concentrations of PEO.

In Figure 5 we plot the onset time and the time for the end of the linear growth regime where the maximum of $\dot{\sigma}$ occurs ($t_{max(\dot{\sigma})}$). Actually, the increase of $t_{max(\dot{\sigma})}$ seems to follow the same behavior as the onset time of the instability. It is clear that the time for the pattern to emerge is greater when the concentration of PEO is higher. This is exactly what was predicted from the pseudo-steady-state linear stability analysis: the time needed for the pattern to emerge comes from the time for the Rayleigh number to be above the pseudo-steady critical Rayleigh number and the time needed for a mode to grow at a sufficient speed. Both quantities increase when the Rayleigh number decreases.[12]

Finally, in Figure 6, we show the evolution in time of the center of the Gaussian fit. It is clear that the evolution is similar in the three cases shown. In the initial stages of the evolution, the wavenumber increases, as predicted by the pseudo-steady-state linear stability analysis.[12] Then at some time the wave-

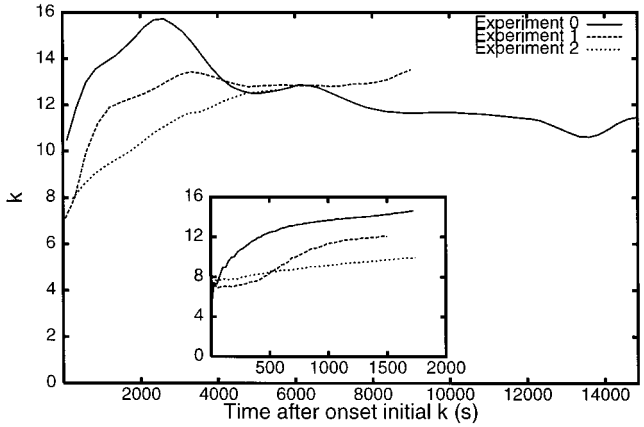

Figure 6. Evolution in time of the center of the Gaussian fit for different initial concentrations of PEO. The time shown in abscissa axis is counted from the time of the first picture, in each experiment, for which the dominant peak of the Fourier spectrum is higher than the noise. The inset shows the evolution at initial stages.

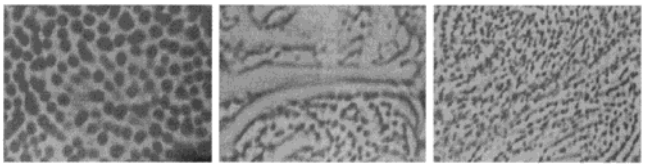

Figure 7. Typical patterns at a time corresponding to the saturation of contrast for increasing initial concentrations of NaOH.

number stops increasing and eventually decrease or stays constant due to nonlinear effects.

In the inset we show the initial stages of the evolution. We see that at the end of this initial stage the higher the concentration of PEO the smaller the dominant wavenumber as it would be expected for a more viscous solution. The system with a lower concentration of PEO, and hence, a higher Rayleigh number is the one which becomes unstable sooner (see Figure 5) and shows the more marked change in the dominant wavenumber. After the onset of the pattern, the corresponding unstable profile still evolves because the chemical reactions are still taking place. The mode which grows faster has increasing wavenumber as this profile evolves. As a consequence, a drift of the dominant wavenumber to higher values is expected and observed in the stages dominated by the linear growth. The case with the highest concentration of PEO (experiment no. 2; see Table 1) has a different behavior. In this case the system becomes unstable later than the cases with lower concentration of PEO. This means that, when the system becomes unstable, the concentration profiles of the compounds are closer to the asymptotic steady state. So, large changes in the profiles do not occur after onset and the mode that is the first to become the fastest growing mode changes slightly during the initial stage.

4.2. Chemical Parameter: pH. In this subsection we discuss the influence of a chemical parameter on the development of the patterns. The chemical species that has the greatest influence on the chemical reaction rates is NaOH,[11] which affects the pH.

The influence of this parameter on the patterns obtained is made evident in Figure 7, where three patterns obtained at three different initial concentrations of NaOH are shown. The time at which these pictures were captured corresponds to saturation of contrast. The most obvious difference in these pictures is the length scale of the structures that form the pattern. The wavenumber grows with increasing initial concentration of NaOH (or pH). The influence on the time scales of the system

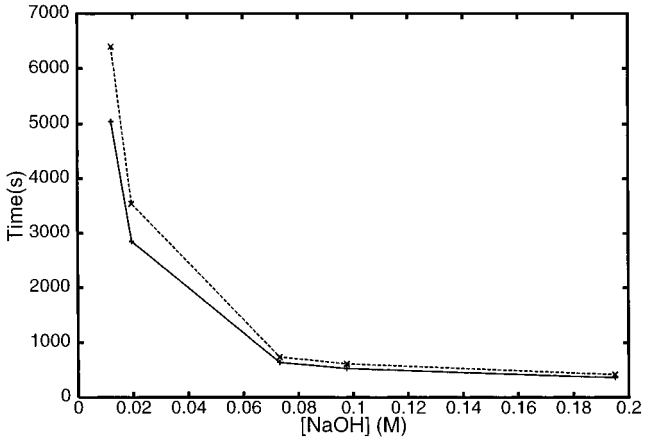

Figure 8. Times for the onset (solid line) and $t_{\max(\dot{\sigma})}$ (dashed line) versus the initial concentrations of NaOH.

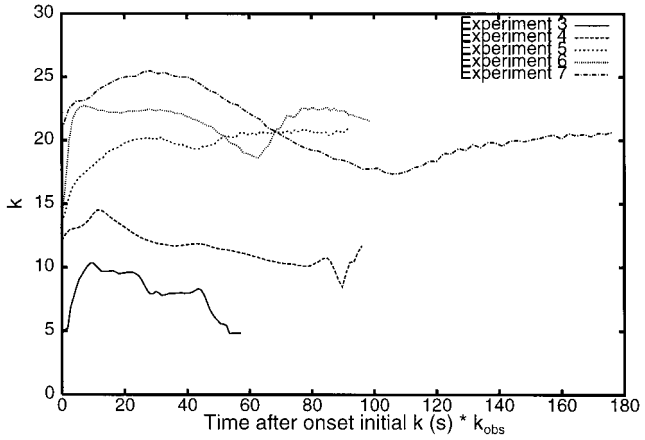

Figure 9. Evolution in time of the center of the Gaussian fit for different initial concentrations of NaOH. The time shown in abscissa axis is counted from the time of the first picture, in each experiment, for which the dominant peak of the Fourier spectrum is higher than the noise. This time has been nondimensionalized using the rate constant of reaction 2. See ref 12.

is large, too. Figure 8 shows the times involved in pattern evolution versus the initial concentration of NaOH. The onset time generally decreases when pH increases. This behavior can be explained by the fact that the reaction rates become larger when the pH of the mixture increases, inducing an early instability. Also, the ratio of the total depth of the fluid to the upper sublayer depth (parameter d) increases (see Table 4) and the system becomes more unstable. On the other hand, the Rayleigh number is decreased (see Table 4) and this stabilizes the system. It appears that the destabilizing effects overcome the stabilizing ones. Furthermore, $t_{\max(\dot{\sigma})}$ decreases with increasing initial [NaOH] following the same behavior as for the onset time.

In Figure 9 we show the evolution in time of the center of the Gaussian fit. The time is nondimensionalized by multiplying by k_{obs} (see ref 12). By doing this we are able to show the evolution of the set of experiments in a similar nondimensional time scale. Again we get the usual behavior: an initial stage where the wavenumber grows, a stage where the wavenumber stops growing, and a final stage where the wavenumber decreases or becomes steady. It is clear that the maximum wavenumber achieved is very dependent on the initial concentration of NaOH. When the value of pH increases and therefore, as indicated above, the more unstable is the system, the dominant wavenumber is higher. In this respect we should also remember

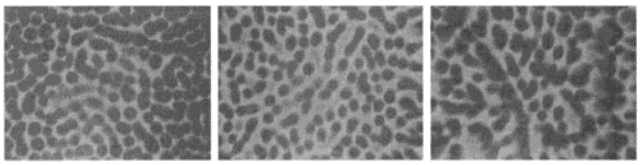

Figure 10. Typical patterns at a time corresponding to the saturation of contrast for increasing layer depth.

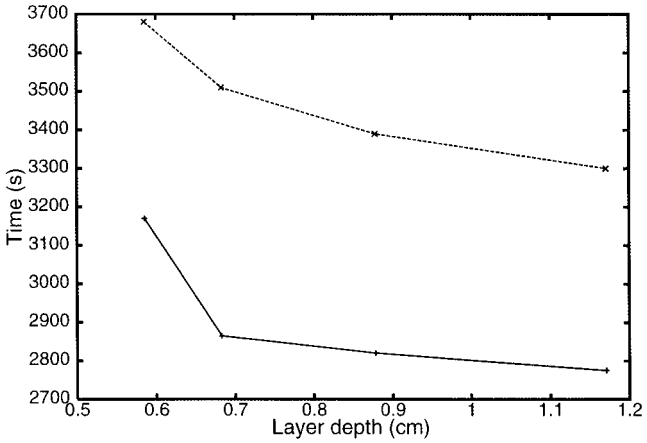

Figure 11. Times for the onset (solid line) and $t_{\max(\dot{\sigma})}$ (dashed line) versus layer depth.

that the length scale of the system used to nondimensionalize the spatial variables in the pseudo-steady-state linear stability analysis $\bar{H} = (D/k_{obs})^{1/2}$ decreases when the rate constant increases.

4.3. Geometrical Parameter: Solution Depth. Finally, we study a geometrical parameter, the solution depth (see Table 4). In Figure 10 we show three examples of patterns at the time corresponding to saturation of σ. It can be seen that the length scales of the system change again significantly. Patterns obtained at layer depths beyond the last example shown have structures which tend to be dominated by lines rather than dots. This transition from dot to line shaped patterns could explain the variability of the experiments conducted at greater depths.

In Figure 11 we show the influence of the layer depth on the time scales involved in the pattern evolution. Both the onset time and the time for the end of the linear growth regime $t_{\max(\dot{\sigma})}$ decrease with increasing layer depth. This is in accordance with the fact that deeper layers are less stable than shallower ones.[12]

In Figure 12 we show the evolution in time of the center of the Gaussian fit at different layer depths. The general behavior follows that described in the two former subsections. First the wavenumber increases, the nonlinear effects stop the mean growth, and then the dominant wavenumber decreases or is maintained (eventually oscillating) until the patterns start to disappear.

In the initial regime the three shallower cases follow a well-defined tendency (see inset). The dominant wavenumber at the emergence of the pattern increases when the layer of the fluid increases. After some evolution this initial trend becomes the opposite one and the dominant wavenumber is higher when the layer is shallower (see patterns shown in Figure 10). This whole behavior is again predicted using the pseudo-steady-state linear stability analysis and can be explained assuming that the dominant mode is the mode one solution which has larger effective wavenumber when the layer is shallower.[12] However, in the last case the behavior is different. It is quite possible that in this case (and in others not shown), the system is subject to

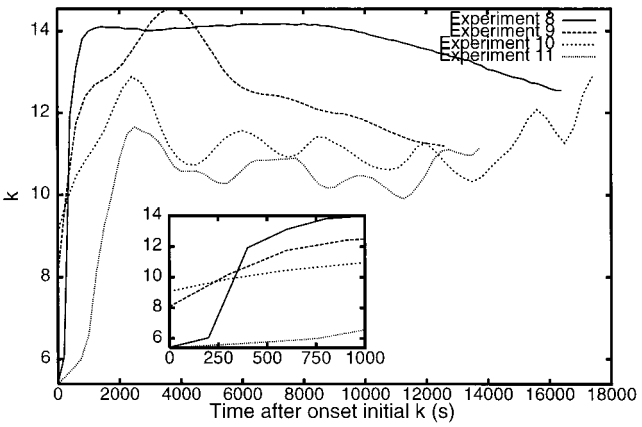

Figure 12. Evolution in time of the center of the Gaussian fit for different layer depths. The time shown in abscissa axis is counted from the time of the first picture, in each experiment, for which the dominant peak of the Fourier spectrum is higher than the noise. The inset shows the evolution at initial stages.

nonlinear modulation at very early stages, or the added depth allows for higher order linear modes.

For the long time behavior, a new interesting feature is displayed by the wavenumber oscillations shown by the two solutions of largest depth (experiment nos. 10 and 11). It seems a common feature that oscillations in the long term appear when the layer is deep. Figure 13 shows more details from experiment no. 11. In part a the complete evolution in time of the Fourier spectrum is displayed. In part b we plot the evolution of the wavenumber distribution. At the initial stages, the dominant wavenumber is close to 5.5, and later, it doubles to 11, being followed by a competition mainly between wavenumbers 8 and 11. This competition lasts for a long time. Another interesting characteristic of this evolution is that the width of the band of excited modes does not decrease so strongly as previous cases (see Figure 3b). In part c we show how the center of the Gaussian fit evolves in time. The "smoothed" oscillations observed in part b can be followed in part c.

5. Conclusions

We have reported experimental measurements that quantify the time and length scales involved in the evolution in time of patterns, formed as a consequence of a chemoconvective instability in the methylene-blue−glucose system.

With image analysis, we have been able to obtain a precise measure of the time of the onset of the pattern and an estimation of the extent of the "linear growth" regime. To study the length scales, we have calculated two-dimensional Fourier transforms. The techniques have been checked by first applying them to a reference case. The quantitative results have been compared, in the appropriate time interval, with the predictions obtained from a linear stability analysis around a pseudo-steady-state.[12] Using the above experimental techniques, we have also studied the quantitative dependence of the chemoconvection patterns on three main control parameters. These parameters are viscosity, pH, and solution depth and correspond to a hydrodynamic, a chemical, and a geometrical parameter, respectively.

We have observed that in the evolution of all the studied cases three main regimes appear. With respect to the dominant pattern wavenumber, the first regime corresponds to linear growth. The second regime consists of an interval where the linear growth is halted and the nonlinear effects become dominant. Finally, the third regime occurs when the evolution in time of the dominant wavenumber no longer has a unique

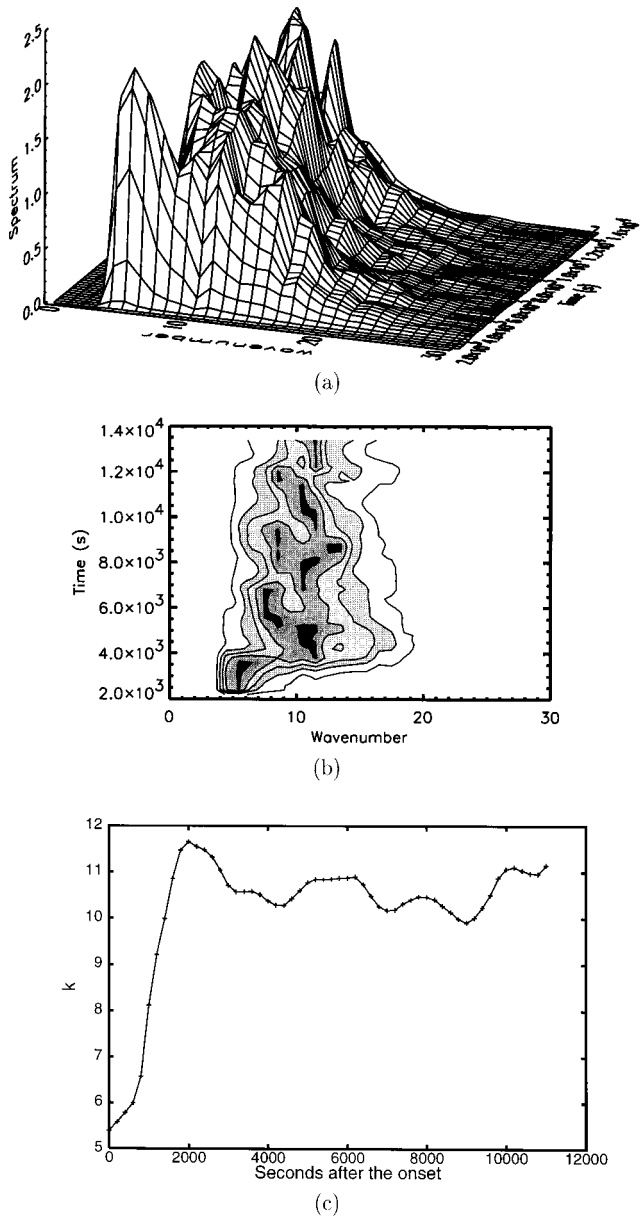

Figure 13. (a) Fourier spectrum versus time from data (experiment no. 11). (b) Levels of gray correspond to 97% (in black), 95%, 90%, 80%, 60%, 40%, and 20% of the highest value of the Fourier spectrum for that time, respectively. (c) Evolution in time of the center of the Gaussian fit to the experimental data. (Here, time 0 means time of the first picture for which the dominant peak of the Fourier spectrum is higher than the noise.) To recover the original time, an offset of 2400 s should be added.

character. During this last regime the dominant wavenumber may either decrease, stay at a steady value or, in some cases, can oscillate around a constant value. The oscillations appear when a competition of coexisting dominant modes is present. These three regimes have been traced, also, by studying the statistics of the gray levels.

With regard to the role of control parameters, we have observed that when the viscosity is increased, the system becomes less unstable, the patterns appear later and their dominant wavenumbers are smaller at the end of the linear growth regime. With respect to the pH, we have found that when it is increased, the system becomes more unstable, the patterns appear after a shorter period of time and the dominant wavenumbers are greater. This control parameter has the greatest influence on both the time and the length scales of the resulting patterns. In both cases, the results obtained in the linear growth regime are in accordance with the general predictions made by the pseudo-steady-state linear stability analysis. Finally, when the layer depth is increased, the system becomes more unstable and the patterns appear within a shorter period of time. The influence of this parameter on the wavenumber evolution is richer than that resulting from the variation of the previous control parameters. In this case, the relationship between pattern wavenumber and layer depth at the very beginning of the linear growth regime is inverted toward its end. Furthermore, patterns resulting from the deepest solutions do not necessarily follow the conclusions above (in general, these examples are not explicitly considered in the present study). The long term behavior changes quantitatively, too, when the solution is sufficiently deep. For a shallow layer, the dominant wavenumber stays steady or decreases slowly. However, when the system is deeper, oscillations in the long-term evolution of the dominant wavenumber appear as a consequence of the competition of several different modes.

Acknowledgment. This work was partially supported by Dirección General de Investigación (DGI) and Comissionat per a Universitat i Recerca (Generalitat de Catalunya) under Projects BXX2000-0638 and 1999-SGR00041 and by the Commission of the European Community within the TMR framework, Grant ERBFMRX-CT96-0085. We express our gratitude to the Danish Natural Science Research Council for a research grand and to European Community-Improving the Human Potential, HPRI-1999-CT-00071. A. J. Pons benefited from a FPU grant from Ministerio de Educación, Cultura y Deporte, reference AP2000-0475, Convocatoria 2000 (B.O.E. 21-11-2000).

References and Notes

(1) Chandrasekhar, S. *Hydrodynamic and Hydromagnetic Stability*; Dover Publications: New York, 1981.
(2) Sharp, D. H. *Phys. D* **1984**, *12*, 3.
(3) DiPrima, R. C.; Swinney, H. L. Instabilities and Transition in Flow between Concentric Rotating Cylinders. In *Hydrodynamic Instabilities and the Transition to Turbulence*; Swinney, H. L., Gollub, J. P., Eds.; Springer-Verlag: New York, 1981.
(4) McCloud, K. V.; Maher, J. V. *Phys. Rep.* **1995**, *260*, 139.
(5) Kapral, R., Showalter, K., Eds. *Chemical Waves and Patterns*; Kluwer: Dordrecht, 1995.
(6) Castets, V.; Dulos, E.; Boissonade, J.; De Kepper, P. *Phys. Rev. Lett.* **1990**, *64*, 2953. Ouyang, Q.; Swinney, H. L. *Nature* **1991**, *352*, 610.
(7) Ben-Jacob, E.; Cohen, I.; Levine, H. *Adv. Phys.* **2000**, *49*, 395.
(8) Murray, J. D. *Mathematical Biology;* Springer-Verlag: Berlin, 1989.
(9) Hill, N. A.; Pedley, T. J.; Kessler, J. O. *J. Fluid Mech.* **1989**, *208*, 509.
(10) Childress, S.; Levandowsky, M.; Spiegel, E. A. *J. Fluid Mech.* **1975**, *69*, 591.
(11) Pons A. J.; Sagués F.; Bees, M. A.; Sørensen P. G. *J. Phys. Chem. B* **2000**, *104*, 2251.
(12) Bees, M. A.; Pons, A. J.; Sørensen, P. G.; Sagués, F. *J. Chem. Phys.* **2001**, *114*, 1932.
(13) Kagan, M. L.; Peleg, S.; Meisels, E.; Avnir, D. Spatial Structures Induced by Chemical Reactions at Interfaces: Survey of Some Possible Models and Computerized Pattern Analysis. In *Lecture Notes in Biomathematics, Modelling of Patterns in Space and Time*; Jäger, W., Murray, J. D., Eds.; Springer-Verlag: Berlin, 1984.
(14) Avnir, D.; Kagan, M. L. *Chaos* **1995**, *5*, 589.
(15) Campbell, J. A. *J. Chem. Educ.* **1963**, *40*, 578.
(16) Adamčíková, L.; Ševčík, P. *J. Chem. Educ.* **1998**, *75*, 1580.
(17) Adamčíková, L.; Pavlíková, K.; Ševčík, P. *Int. J. Chem. Kinet.* **1999**, *31*, 463.
(18) Adamčíková, L.; Ševčík, P. *Z. Naturforsch. A* **1997**, *52*, 650.
(19) Vandaveer, W. R., IV; Mosher, M. *J. Chem. Educ.* **1997**, *74*, 402.
(20) Bees, M. A.; Hill, N. A. *J. Exp. Biol.* **1997**, *200*, 1515.
(21) Czirók, A.; Jánosi, I. M.; Kessler, J. O. *J. Exp. Biol.* **2000**, *203*, 3345.
(22) Jánosi, I. M.; Kessler, J. O.; Horváth V. K. *Phys. Rev. E* **1998**, *58*, 4793.
(23) Chapman C. J.; Proctor M. R. E. *J. Fluid Mech.* **1980**, *101*, 759.